A Mechanism for Atmospheric Regime Behavior

D. T. CROMMELIN[*]

Royal Netherlands Meteorological Institute, De Bilt, and Department of Mathematics, Utrecht University, Utrecht, Netherlands

J. D. OPSTEEGH

Royal Netherlands Meteorological Institute, De Bilt, and Institute for Marine and Atmospheric Research, Utrecht University, Utrecht, Netherlands

F. VERHULST

Department of Mathematics, Utrecht University, Utrecht, Netherlands

ABSTRACT

Adopting the viewpoint that atmospheric flow regimes can be associated with steady states, this work investigates the hypothesis that regime transitions in deterministic atmosphere models are related to the existence of heteroclinic connections between these steady states. A low-order barotropic model with topography is studied, in which topographic and barotropic instabilities are the mechanisms dominating the dynamics. By parameter tuning, the Hopf bifurcation corresponding to barotropic instability can be made to coincide with one of the saddle-node bifurcations that are due to the topography in the model. This coincidence is called a fold-Hopf bifurcation. Among the dynamical structures related to such a bifurcation are heteroclinic connections and homoclinic orbits, connected to the equilibria. A heteroclinic cycle back and forth between the equilibria, existing in the truncated normal form of the fold-Hopf bifurcation, will be perturbed in the full model, leaving orbits homoclinic to one of the equilibria. The impact of these mathematical structures explains several characteristics of regime behavior known from previous model studies.

1. Introduction

More than 50 years after the first reports on the topic, the regime behavior of the atmosphere remains an enigma. The considerable attention that has been devoted to the hypothesis that atmospheric low-frequency variability is affected by the existence of preferred flow regimes has not yet resulted in a fully conclusive picture. Nevertheless, the detection of regimes in the observational data of the atmosphere has progressed significantly in the last two decades. Starting with Benzi et al. (1986) and Sutera (1986), the somewhat intuitive notion of regimes, developed since the works of Namias (1950) and Rex (1950a,b), was put on a firmer basis using concepts and techniques from modern probability theory. In papers such as Cheng and Wallace (1993),

Kimoto and Ghil (1993a,b), Smyth et al. (1999), and Monahan et al. (2001), the use of these techniques has resulted in growing evidence for the existence of regimes in Northern Hemisphere atmosphere data. Moreover, the regimes found in these papers, using different techniques, are strikingly similar.

Accepting the existence of regimes still leaves us with the question of which dynamical processes are responsible for this behavior. An important contribution regarding this issue was made by Charney and DeVore (1979, hereafter CDV), who stated that flow regimes should be identified with equilibrium solutions of the equations describing the evolution of large-scale atmospheric flow. Their hypothesis, supported by the study of a low-order model for barotropic flow over topography, was taken up and expanded on by, among others, Reinhold and Pierrehumbert (1982), Legras and Ghil (1985), Källén (1981, 1982), Yoden (1985), De Swart (1988a,b, 1989), and Itoh and Kimoto (1996, 1999).

Although the earlier-mentioned model studies unveiled much about the structure of the (model) regimes, the observed regime transitions have so far not been satisfactorily explained. From statistical studies of mod-

* Current affiliation: Courant Institute of Mathematical Sciences, New York University, New York, New York.

Corresponding author address: D. T. Crommelin, Courant Institute of Mathematical Sciences, New York University, New York, NY 10012-1185.
E-mail: crommelin@cims.nyu.edu

el data as well as observational data, it has been known for some time that transitions between regimes are not an entirely random process. In Mo and Ghil (1987, 1988), Molteni et al. (1990), and Kimoto and Ghil (1993b), up to seven regimes/clusters are identified in various datasets (both from observations and models). By counting the transitions between the various regimes, these studies made clear that there exist not only preferred flow regimes, but also preferred transitions between (some of) the regimes. Plaut and Vautard (1994), studying the interplay between low-frequency oscillations and regimes using multichannel singular spectrum analysis (MSSA), also found that transitions are not purely random.

Itoh and Kimoto (1996, 1997, 1999) propose chaotic itinerancy as an explanation for the preferences and inhomogeneities in regime transitions. Using multilayer quasi-geostrophic models of moderate complexity (L2T15 and L5T21), they detect multiple attractors that are identified as regimes. By changing a parameter (horizontal diffusivity or static stability), these attractors lose their stability one by one, thereby admitting regime transitions. When all attractors have lost their stability, the model shows irregular transitions between the remnants of the former attractors, and thus between the regimes. This behavior is called chaotic itinerancy. The preferred order of the transitions is related to the order in which the attractors lost their stability. This interesting result once more emphasizes the inhomogeneities in regime transitions, which must be due to the nonlinear nature of the system under study. However, it does not provide much insight into the dynamics that determine the transitions, as the loss of stability of the various attractors is not analyzed. It remains unknown what dynamical processes cause and drive the transitions.

Often a stochasticity assumption is invoked to explain regime transitions. Noise, representing the effect of unresolved physics and dynamics, can kick a system out of the basin of attraction of one regime and into another. This has been studied by adding stochastic perturbations to a low-order model (e.g., Egger 1981, Benzi et al. 1984, De Swart and Grasman 1987, and Sura 2002). However, the addition of noise is not necessary to trigger regime transitions. Even in deterministic low-order models transitions can occur. It is therefore worthwhile to consider how transitions can be generated by the internal, deterministic dynamics of a system, in the absence of noise.

Our hypothesis will be that barotropic flow over topography is not only sufficient to create multiple equilibria (as in CDV), but can also generate transitions between those equilibria, resulting in regime behavior. This is based on the fact that transitions have been observed in various barotropic models. Examples are the 25-variable model used by Legras and Ghil (1985), the 10-dimensional model used by De Swart (1988a,b), and the T21 model studied in Crommelin (2003b). The presence of baroclinic processes is apparently no conditio

sine qua non for regime transitions. Recently, even in laboratory experiments designed to mimic as closely as possible the situation of barotropic flow over topography in the atmosphere, regime behavior was observed (Weeks et al. 1997; Tian et al. 2001). Thus, the transitions found in several truncated barotropic models cannot simply be discarded as model artifacts.

In Crommelin (2003b) strong numerical evidence was found in support of the hypothesis that remnants of heteroclinic connections are responsible for the transitions between flow regimes. The regimes were found to correspond with steady states, in accordance with the paradigm introduced by CDV, and are likely to have deterministic connections running back and forth between them for nearby parameter values. An attempt was made to find the trajectories of the connections, and the result of that attempt was shown to be consistent with the phase space preferences of regime transitions during a 200-yr model integration. In spite of the numerical evidence, analytical, or at least more rigorous mathematical support is still lacking for the hypothesis that regime transitions are related to heteroclinic connections [a hypothesis also mentioned by Legras and Ghil (1985), Kimoto and Ghil (1993b) and Weeks et al. (1997)]. In this paper we want to provide such support, by studying a low-order model of the atmospheric flow at midlatitudes. We hypothesize that the combination of topographic and barotropic instability is sufficient to create multiple equilibria corresponding to regimes as well as connections between these equilibria, and we therefore take the simplest model possible that combines these two instability mechanisms. Such a model is provided by De Swart (1989, hereafter DS), a six-variable model that is essentially the same as the model of CDV, also studied by Yoden (1985), except for a different scaling and a more general zonal forcing profile. We will use this model to study the interaction between topographic and barotropic instability, in order to see if and how the combination of these instability mechanisms can generate connections between steady states, resulting in regime behavior.

The study of this interaction can provide a first step toward a better understanding of the mechanisms playing a role in the phenomenon of regime transitions. Although the model that will be used is probably too simple to arrive at conclusions that pertain immediately to the real atmosphere, the insights it provides may guide the investigation of more complex models, or even observational data.

2. Derivation of the low-order model

The starting point for this study is the hypothesis that the combination of topographic and barotropic instability is sufficient to generate regime behavior. Notably, baroclinic processes are not considered to be truly necessary for regime transitions to occur. Thus, we consider a model without baroclinic dynamics and without sto-

chastic terms supposed to represent the effect of baroclinic processes. Instead, we wish to study the simplest deterministic model possible that combines the mechanisms of barotropic and topographic instability. Therefore we use the model presented in DS, a slightly different version of the CDV model. It can have multiple equilibria, caused by topography, and is forced by a zonal flow profile that can be barotropically unstable.

The model is obtained by a Galerkin projection and truncation of the barotropic vorticity equation (BVE) on a β-plane channel. The BVE, a partial differential equation, reads

$$\frac{\partial}{\partial t}\nabla^2\psi = -\mathcal{J}(\psi, \nabla^2\psi + f + \gamma h) - C\nabla^2(\psi - \psi^*).$$

(2.1)

Time (t), longitude (x), and latitude (y) can take on values $(t, x, y) \in \mathbb{R} \times [0, 2\pi] \times [0, \pi b]$. The parameter $b = 2B/L$ determines the ratio between the dimensional zonal length L and meridional width B of the channel. The streamfunction field $\psi(t, x, y)$ is periodic in x: $\psi(t, x, y) = \psi(t, x + 2\pi, y)$. The restriction to the beta plane implies that at the meridional boundaries $y = 0$, π both $\partial\psi/\partial x = 0$ and $\int_0^{2\pi}(\partial\psi/\partial y)\,dx = 0$. The Coriolis parameter f generates the beta effect in the model. Orography enters with h, the orographic height, and is scaled with γ. The Jacobi operator $\mathcal{J}$ acts on two fields, say $A(x, y)$ and $B(x, y)$, as follows: $\mathcal{J}(A, B) = (\partial A/\partial x)(\partial B/\partial y) - (\partial A/\partial y)(\partial B/\partial x)$. Finally, the model is driven by a Newtonian relaxation to the streamfunction profile ψ^*, with damping coefficient C.

To arrive at a finite-dimensional model, the BVE is projected onto a set of basis functions which are eigenfunctions of the Laplace operator ∇^2. On the chosen rectangular domain, with the earlier-mentioned boundary conditions, these functions are double Fourier modes:

$$\phi_{0m}(y) = \sqrt{2}\,\cos(my/b)$$

$$\phi_{nm}(x, y) = \sqrt{2}e^{inx}\sin(my/b),$$ (2.2)

in which $|n|, m = 1, 2, \ldots,$. The streamfunction and the topographic height are expanded in this basis

$$\psi(t, x, y) = \sum_{n,m}\psi_{nm}(t)\phi_{nm}, \qquad h(x, y) = \sum_{n,m}h_{nm}\phi_{nm}.$$

(2.3)

The six-dimensional model is obtained by truncating the expansion after $|n| = 1$ and $m = 2$, so the only remaining basis functions are ϕ_{01}, ϕ_{02}, ϕ_{11}, ϕ_{-11}, ϕ_{12}, and ϕ_{-12}. The time-dependent variables ψ_{01}, ψ_{02}, $\psi_{\pm11}$, $\psi_{\pm12}$ are transformed to real variables:

$$x_1 = \frac{1}{b}\psi_{01}, \qquad x_2 = \frac{1}{b\sqrt{2}}(\psi_{11} + \psi_{-11}),$$

$$x_3 = \frac{i}{b\sqrt{2}}(\psi_{11} - \psi_{-11}),$$

$$x_4 = \frac{1}{b}\psi_{02}, \qquad x_5 = \frac{1}{b\sqrt{2}}(\psi_{12} + \psi_{-12}),$$

$$x_6 = \frac{i}{b\sqrt{2}}(\psi_{12} - \psi_{-12}).$$ (2.4)

The topography h is chosen to have a (1, 1) wave profile:

$$h(x, y) = \cos(x)\sin(y/b),$$ (2.5)

so the only nonzero topographic expansion coefficients are $h_{11} = h_{-11} = 1/(2\sqrt{2})$. The forcing profile ψ^*, finally, is purely zonal, that is $\psi^* = \psi^*(y)$. For the 6D model this means that the only forcing terms will be x_1^* and x_4^*.

The set of ordinary differential equations describing the temporal evolution of the x_i is of the form $\dot{\mathbf{x}} = \mathbf{F} + A\mathbf{x} + B(\mathbf{x}, \mathbf{x})$, with energy- and enstrophy-preserving quadratic nonlinearities. In detail it reads

$$\dot{x}_1 = \tilde{\gamma}_1 x_3 - C(x_1 - x_1^*)$$

$$\dot{x}_2 = -(\alpha_1 x_1 - \beta_1)x_3 - Cx_2 - \delta_1 x_4 x_6$$

$$\dot{x}_3 = (\alpha_1 x_1 - \beta_1)x_2 - \gamma_1 x_1 - Cx_3 + \delta_1 x_4 x_5$$

$$\dot{x}_4 = \tilde{\gamma}_2 x_6 - C(x_4 - x_4^*) + \varepsilon(x_2 x_6 - x_3 x_5)$$

$$\dot{x}_5 = -(\alpha_2 x_1 - \beta_2)x_6 - Cx_5 - \delta_2 x_4 x_3$$

$$\dot{x}_6 = (\alpha_2 x_1 - \beta_2)x_5 - \gamma_2 x_4 - Cx_6 + \delta_2 x_4 x_2.$$ (2.6)

The various coefficients in these equations are given by

$$\alpha_m = \frac{8\sqrt{2}}{\pi}\frac{m^2}{4m^2 - 1}\frac{b^2 + m^2 - 1}{b^2 + m^2},$$

$$\beta_m = \frac{\beta b^2}{b^2 + m^2},$$

$$\delta_m = \frac{64\sqrt{2}}{15\pi}\frac{b^2 - m^2 + 1}{b^2 + m^2},$$

$$\tilde{\gamma}_m = \gamma\frac{4m}{4m^2 - 1}\frac{\sqrt{2}b}{\pi},$$

$$\varepsilon = \frac{16\sqrt{2}}{5\pi},$$

$$\gamma_m = \gamma\frac{4m^3}{4m^2 - 1}\frac{\sqrt{2}b}{\pi(b^2 + m^2)}.$$ (2.7)

In the equations, the terms multiplied by α_i model the advection of the waves by the zonal flow. The β_i terms are due to the Coriolis force; the γ terms are generated by the topography. The C terms take care of the Newtonian damping to the zonal profile $x^* = (x_1^*, 0, 0, x_4^*, 0, 0)$. The δ- and ε-terms describe the nonlinear triad interaction between the zonal (0, 2) mode and the (1, 1) and (1, 2) waves. This triad is responsible for the possibility of barotropic instability of the (0, 2) mode.
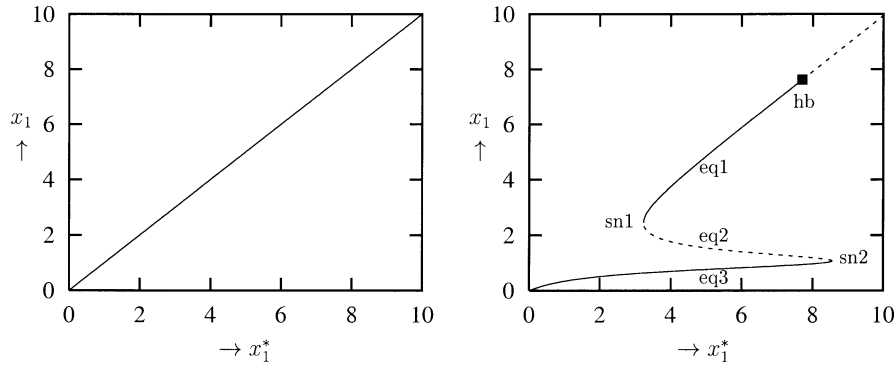
FIG. 1. Continuation of fixed points. Solid lines denote stable branches and dashed lines unstable branches. (left) Barotropic instability is not possible and topography is zero ($r = \gamma = 0$). (right) Topography is nonzero ($\gamma = 1$), generating two saddle-node bifurcations (sn1 and sn2). The three branches of equilibria are denoted by eq1, eq2, and eq3. The Hopf bifurcation hb (solid square) is due to barotropic instability ($r = -0.4$).

The number of free parameters in the model equations is six: the damping coefficient C, the forcing parameters x_1^* and x_4^*, the length–width ratio of the beta channel, b, the beta-effect parameter β, and the scaling of the topographic height γ. In the analysis of this paper we will most of the time use the ratio r between x_4^* and x_1^* as a free parameter instead of x_4^* itself. This is done by putting $x_4^* = rx_1^*$.

The model parameters x_1^*, x_4^* (or r) and γ will be varied throughout this study. The remaining parameters β, b, and C will be kept fixed. The choice $\beta = 1.25$ corresponds to a channel centered around a latitude of 45°, see also DS. In DS, C was set to 0.1, corresponding to a damping time scale of 10 days (the nondimensional time in the equations was scaled such that $\Delta t = 1$ corresponds to roughly 1 day). We will adopt the same value for C.

The channel width–length ratio b will be set to 0.5, which is different from the value taken throughout most of the study of DS. There, $b = 1.6$ was chosen. However, at that value the model contains pitchfork bifurcations that create additional branches of equilibria. Since we want to isolate the mechanisms of barotropic and topographic instability in their simplest form, such additional bifurcations are unwanted. By choosing $b = 0.5$ (i.e., reducing the north–south extent of the channel from 80% to 25% of its east–west extent) these extra pitchfork bifurcations do not occur. This value of b is not unphysical, considering that the east–west extent of the midlatitude regions on earth is a lot larger than their north–south extent. Moreover, since regime behavior is a low-frequency variability phenomenon, it is associated with planetary scales rather than synoptic scales. The planetary waves are not isotropic; in longitudinal direction their wavelength is much larger than in meridional direction.

3. Topographic and barotropic instability

Nonzero topography may introduce a mechanism of instability in the system. The interaction between the zonal flow and the topography can generate standing wave solutions. The (0, 1) zonal flow component will excite a wave with the same wavenumber as the topography, in this case the (1, 1) wave. The effect of the topography does not end there; as can be seen in the equations, the (1, 2) wave mode is coupled to the (0, 2) zonal mode via the topography. It must be pointed out that the topography does not create an oscillatory mode (as is usually the case with instabilities), but rather a resonant response curve which corresponds to a parameter range with multiple equilibria. These equilibria are associated with three different ways in which the advection of relative vorticity, the advection of planetary vorticity, and the vortex stretching caused by flow over topography can balance. One of the equilibria is unstable. Since the instability of this steady state is entirely due to the topography, and not to other mechanisms such as barotropic instability or wave instability, the effect of the topography here has been given a new name, topographic instability.

The barotropic instability is an instability mechanism in the more common sense of the word, as it refers to a situation where a steady state (a mainly zonal flow) loses its stability while a (stable) oscillatory wave mode (a travelling wave) is created. The zonal flow profile must obey certain conditions for this instability to be possible (see, e.g., Kuo 1949 and Cushman-Roisin 1994). In particular, the profile must have at least one inflection point (a change in the sign of the total vorticity) in meridional direction. For that reason it is necessary to have more zonal modes resolved in the model, since the (0, 1) zonal mode can never be barotropically unstable by itself (it does not obey the inflection point condition). The (0, 2) zonal mode can become unstable, though only when $b^2 < 3$, due to Fjørtofts theorem (see DS). Our choice of $b = 0.5$ clearly satisfies this condition.

The effect of the two mechanisms is shown in Fig. 1. On the left is a curve of fixed points depicted in the
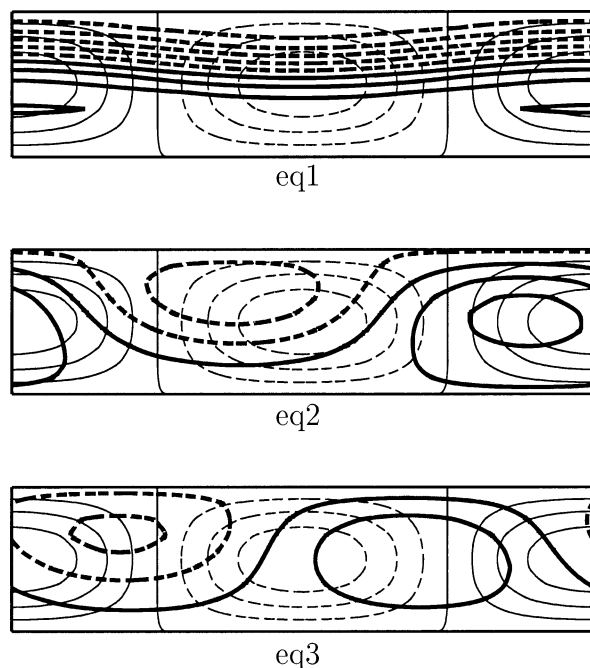
FIG. 2. Streamfunction patterns corresponding to the equilibria at $x_1^* = 6$, $r = -0.4$, $\gamma = 1$. (top and bottom) The stable equilibria; (middle) the unstable one. Thick lines are streamfunction lines (contour interval 1 in nondimensional units), thin lines are topography contours (interval 0.25 km). Dashed lines/contours are for negative values, solid lines/contours for zero or positive values.

FIG. 3. Location of cusp bifurcation for varying γ and r. The value of x_1^* also changes along the curve but is not shown.

situation without either mechanism playing a role. This was achieved by putting $\gamma = x_4^* = 0$, so that topography is zero and the zonal flow profile cannot be barotropically unstable. The response of the model to varying x_1^* is a shift of the steady state such that $x_1 = x_1^*$. On the right, both mechanisms are present. The deformation of the straight curve on the left to the S-shaped curve on the right, involving two saddle-node bifurcations (sn1 and sn2), is the result of nonzero topography ($\gamma = 1$). The (supercritical) Hopf bifurcation on the upper part of the branch represents the barotropic instability, which was triggered by nonzero x_4^*. To be able to perform fixed-point continuations starting with zero flow (all $x_i = 0$) at zero forcing, x_4^* is scaled with x_1^*, by putting $x_4^* = rx_1^*$ and fixing r at some value (thus, r then controls the shape of the forcing profile while x_1^* determines its strength). This scaling will be used throughout this paper. In Fig. 1, right, $r = -0.4$ was taken. The continuations were carried out using the software package AUTO (Doedel and Wang 1995).

The flow patterns corresponding to the three different fixed points existing at $x_1^* = 6$ in Fig. 1 are shown in Fig. 2. As was already known from previous studies (e.g., DS), the upper branch eq1 corresponds to equilibria with largely zonal character. The other two are dominated by topographically excited standing wave patterns, one superresonant (eq2), the other subresonant (eq3). The former has a slightly stronger zonal flow
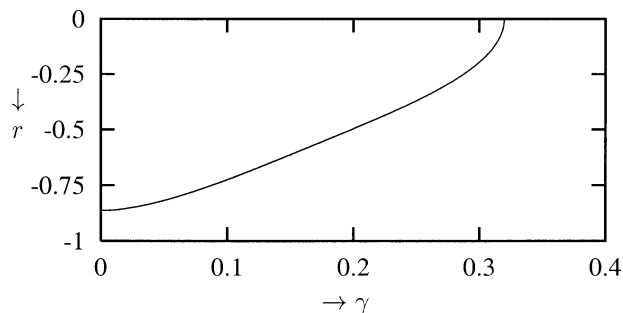
component than the latter. The phases of their wave components with respect to the topography are somewhat different: the wave pattern of eq3 is a bit more upstream than that of eq2. The phase difference goes to 0 when moving toward sn2.

The subresonant solution eq3 is usually the one that is identified as the regime of blocked flow. The main reason for that seems to be the fact that in the simplest setting (i.e., topographic instability being the only physical mechanism present) eq3 is the stable solution, whereas eq2 is unstable. Nevertheless, eq2 also possesses the characteristics of a blocked flow regime. To call eq2 an intermediate solution only because it is unstable in the simple setting seems premature. Eventually, all equilibria have to be unstable for regime transitions to occur in a model without stochastic terms. We see no a priori reason to exclude eq2 as a candidate for the blocked regime.

4. The merging of two instabilities: A fold-Hopf bifurcation

a. Instabilities and bifurcations

The two instabilities are, mathematically, represented by saddle-node and Hopf bifurcations. The locations of these bifurcations depend on the parameters of the model. Figure 1 already gave an idea of this dependence. The straight curve of fixed points, where the equilibrium is such that the dissipation and the forcing of the first zonal mode are in balance, gets deformed by increasing the amplitude of the topography above some threshold value. At the threshold value, the two saddle-node bifurcations sn1 and sn2 coincide. Thus, the threshold is a cusp bifurcation. The cusp is a codimension-2 bifurcation (two parameters, say x_1^* and γ, must be tuned for this bifurcation to occur) and can be continued adding a third parameter, say r. This means that the value of γ for which the cusp occurs changes when altering the shape of the zonal forcing. A curve showing the γ location of the cusp for varying r is drawn in Fig. 3. It must be stressed that the value of x_1^* for which the cusp occurs also changes along the curve: it decreases monotonically from $x_1^* = 1.992$ at $\gamma = 0.3198$ to $x_1^* = 0.3320$

at $\gamma = 3.0 \times 10^{-12}$. The continuation of the cusp was performed using the continuation software package CONTENT (Kuznetsov and Levitin 1997). Note that if the zonal forcing profile has the right shape and strength ($x_1^* = 0.3320$, $r = -0.861467$), the influence of the topography is even felt when its amplitude is infinitesimally small (γ approaching zero).

The Hopf bifurcation is the dynamical expression of barotropic instability. Since the $(0, 2)$ zonal mode can become barotropically unstable but the $(0, 1)$ mode cannot, it can be expected that the bifurcation occurs at smaller x_1^* values if $|r|$ is increased. By doing so, the Hopf bifurcation will approach the saddle-node sn1, and at some point coincide with it. This simultaneous occurrence of a saddle-node (or fold) and a Hopf bifurcation is called a fold-Hopf bifurcation, and has codimension 2.

Let us investigate what happens when this fold-Hopf bifurcation occurs (i.e., when the two instability mechanisms merge). The description of the various dynamical phemonena and structures that emerge out of this codimension two point in parameter space, the so-called unfolding of the bifurcation, is given in Kuznetsov (1995). We will briefly review it here.

b. The fold-Hopf bifurcation: Some theory reviewed

The occurrence of a bifurcation of a fixed point can be read off from the eigenvalue-spectrum of the fixed point. In a saddle-node (or fold) bifurcation, one eigenvalue is exactly zero, all the others have nonzero real parts. In a Hopf bifurcation, one complex conjugated pair of eigenvalues has a real part zero (and an imaginary part nonzero); again, all other eigenvalues are bounded away from the imaginary axis. It will come as no surprise that a fold-Hopf bifurcation is characterized by a fixed-point eigenvalue spectrum with one zero and one purely imaginary pair (i.e., $\lambda_1 = 0$, $\lambda_{2,3} = \pm i\omega$) as its only eigenvalues on the imaginary axis. The fold-Hopf bifurcation is sometimes also referred to as zero-Hopf, zero-pair, or Gavrilov–Guckenheimer bifurcation.

Suppose we have an n-dimensional system depending on p parameters

$$\dot{x} = f(x, \mu), \qquad x \in \mathbb{R}^n, \qquad \mu \in \mathbb{R}^p, \quad (4.1)$$

with fixed point $x = x_0$ at $\mu = \mu_0$ [so $f(x_0, \mu_0) = 0$]. If μ_0 is a fold-Hopf bifurcation point, the eigenvalue spectrum contains n_- eigenvalues λ_i^- with negative real part, n_+ eigenvalues λ_i^+ with positive real part and finally one zero and one imaginary pair: $\mathrm{Re}\lambda_1^-, \ldots, \lambda_{n-}^- < 0 < \mathrm{Re}\lambda_1^+, \ldots, \lambda_{n+}^+$; $\lambda_1^0 = 0$, $\lambda_{2,3}^0 = \pm i\omega$. Clearly, $n_- + n_+ + 3 = n$. We will denote the linear eigenspaces corresponding to the three groups $\{\lambda_i^-\}$, $\{\lambda_i^+\}$, $\{\lambda_i^0\}$ by E^-, E^+, and E^0, respectively: the stable, the unstable, and the *center* eigenspace. The Center Manifold Theorem states that there exists a (only locally defined) three-dimensional invariant manifold W^c that is tangent to E^0 in x_0. The only interesting dynamics of the system

in the neighborhood of x_0 takes place on W^c. Away from W^c, the system is either exponentially fast repelled from W^c (along the unstable manifold) or attracted toward W^c (along the stable manifold), and thus "trivial." W^c is called the center manifold.

The dynamics of the system around x_0 can be described (apart from the exponentially fast repelling and/or attracting to W^c) by the dynamics on the center manifold. Thus, to understand the (local) behavior of the system in and near a fold-Hopf bifurcation, we can restrict ourselves by looking at the center manifold dynamics. A nonlinear, parameter-dependent transformation of variables allows us to isolate the description of the system on W^c (a so-called center manifold reduction). The equations describing the evolution on W^c can be cast in a standardized form; this is called the normal form. We will not discuss the way to calculate the normal form and the center manifold reduction, see Kuznetsov (1995, 1999) for a detailed discussion. Instead, we only give the normal form of the fold-Hopf bifurcation:

$$\dot{y} = \rho_1 + y^2 + s|z|^2 + O(|y, z, \bar{z}|^4)$$

$$\dot{z} = (\rho_2 + i\omega_1)z + (\theta + i\vartheta)yz + y^2z + O(|y, z, \bar{z}|^4).$$

$$(4.2)$$

Here, $y \in \mathbb{R}$ and $z \in \mathbb{C}$; ρ_1 and ρ_2 are called the unfolding parameters, ω_1, θ, and ϑ are coefficients whose values depend on ρ_1 and ρ_2, and $s = +1$ or -1. We assume $\theta \neq 0$ when $\rho_1 = \rho_2 = 0$. The fold-Hopf bifurcation point is at $(\rho_1, \rho_2) = (0, 0)$. There, the normal form equations have a fixed point $y = z = 0$ with eigenvalue spectrum 0, $\pm i\omega_1$.

Truncating the normal form after the cubic terms and transforming z to polar coordinates, $z = ue^{i\phi}$, yields

$$\dot{y} = \rho_1 + y^2 + su^2 \qquad \dot{u} = (\rho_2 + \theta y + y^2)u$$

$$\dot{\phi} = \omega_1 + \vartheta y. \qquad (4.3)$$

This system is called the truncated normal form. As can be seen, the equations for y and u do not depend on ϕ. Moreover, in the neighborhood of the fixed point, $\dot{\phi} \approx \omega_1$, due to small y. The bifurcations in the preceding system can therefore be understood by only studying the equations for y and u, the so-called (truncated) amplitude equations. Note that the truncated amplitude equations are $\mathbb{Z}_2$-symmetric, as they are invariant under $u \to -u$. See Kuznetsov (1995) for a discussion. This symmetry is related to the S^1-symmetry (invariance under $\phi \to \phi + \phi_c$ for arbitrary constants ϕ_c) of the truncated normal form.

Qualitatively, the bifurcation diagram near the origin in the (ρ_1, ρ_2) plane is determined by the signs of s and θ. There are four different cases, or unfolding scenarios. Which scenario applies to our situation can be deduced from the fact that in our system the Hopf bifurcation, when it is located on the upper, stable branch, is supercritical: the stable equilibrium loses its stability while
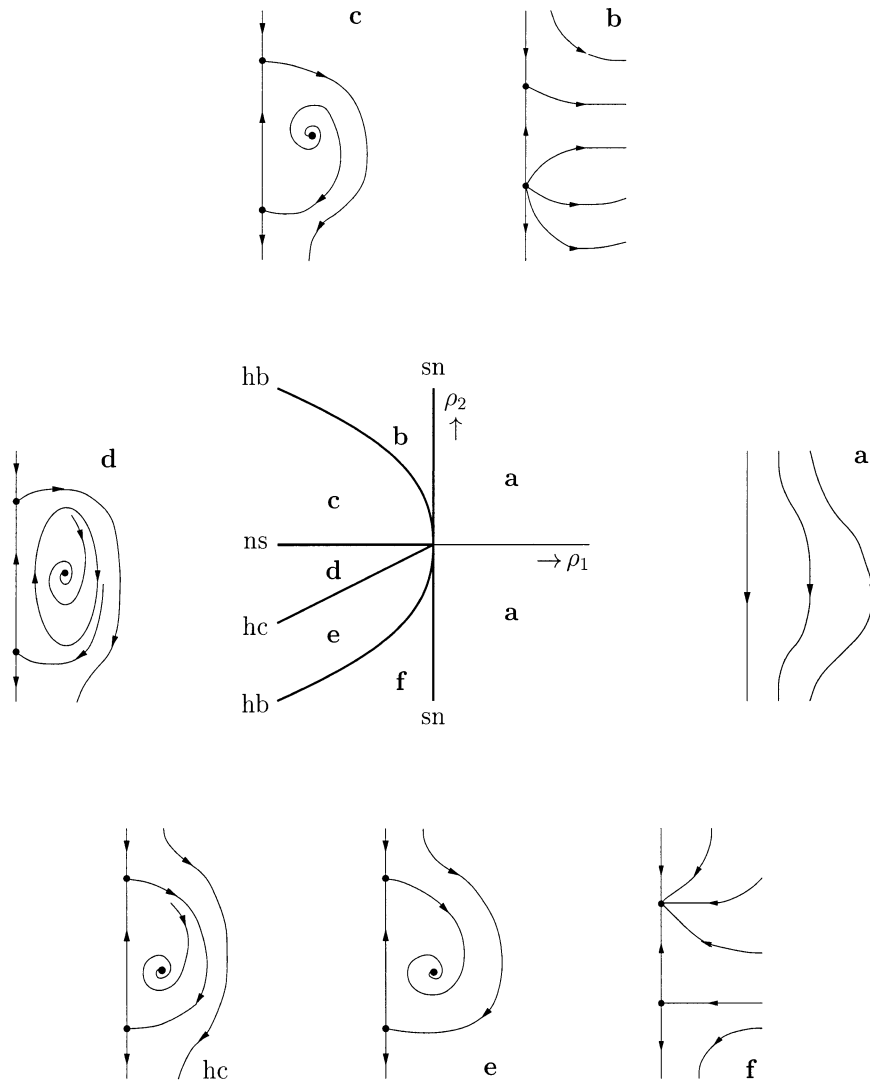
FIG. 4. Bifurcation diagram of the truncated amplitude equations of the fold-Hopf bifurcation with $s = 1$, $\theta < 0$. The various lines and curves in the diagram are denoted hb for Hopf bifurcation, hc for heteroclinic cycle, ns for Neimark–Sacker bifurcation, and sn for saddle-node bifurcation. The seven phase portraits (a)–(f) and hc show the dynamics in the (u, y) plane.

a stable periodic solution is created. It leaves the scenario with normal-form coefficients $s = 1$, $\theta < 0$ as only possibility. This can be checked by continuation of the Hopf bifurcation using (a not yet publicly available version of) CONTENT, which calculates the normal-form coefficients when the Hopf bifurcation curve crosses a fold-Hopf point. Indeed it is found that $s = 1$, $\theta < 0$.

We will not discuss all four unfolding scenarios but restrict ourselves to the one relevant for this study. The bifurcation diagram for the truncated normal form in case $s = 1$, $\theta < 0$ is shown in Fig. 4, together with phase portraits in the (u, y) plane for the various regions of the diagram. In origin of the (ρ_1, ρ_2) plane we find the fold-Hopf point. From the origin, a saddle-node line sn ($\rho_1 = 0$) and a Hopf curve hb [$\rho_1 = -\rho_2^2/\theta^2 + o(\rho_2^2)$]

emanate. For $\rho_1 > 0$ no equilibria or periodic orbits exist. When crossing sn, two equilibria are created. The invariance of the line $u = 0$ (or, equivalently, $z = 0$) in the truncated normal form guarantees the existence of a heteroclinic connection on the y axis between the two equilibria.

When crossing hb, one of the equilibria (which one depends on the sign of ρ_2) undergoes a Hopf bifurcation. The periodic orbit born on the Hopf curve encounters a Neimark–Sacker bifurcation (also called torus bifurcation) when crossing the line $\rho_2 = 0$, $\rho_1 < 0$. The Neimark–Sacker line, denoted ns, also emanates from the origin of the parameter plane. Note that in the truncated amplitude equations a Hopf bifurcation actually appears as a fixed point moving into the $u > 0$ plane. A fixed point of the truncated amplitude equations with
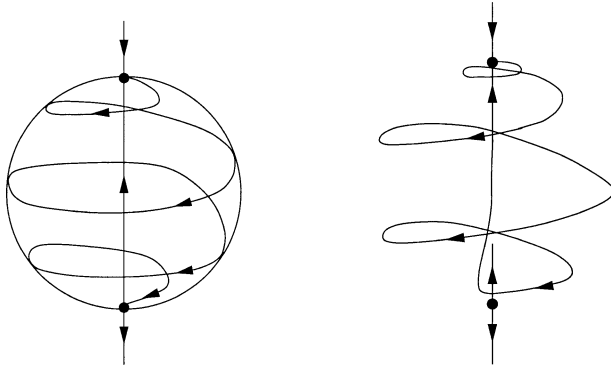
FIG. 5. (left) Spherelike heteroclinic cycle between two equilibria. The cycle exists on curve hc of the truncated normal form (4.3). (right) One of the homoclinic orbits remaining after adding perturbative higher-order terms to the truncated normal form.

FIG. 6. (top) Bifurcation diagram with fold-Hopf bifurcation (fh) as guiding center; includes the saddle-node bifurcation curves sn1 and sn2 (coming together in the cusp bifurcation c), the Hopf bifurcation curve hb, and the period-doubling curve pd. The thin solid line winding in toward the fold-Hopf point is the homoclinic bifurcation curve ho. (bottom) In the magnification the curve of the Neimark-Sacker (or torus) bifurcation ns is visible: it emanates from the fh point and ends on the pd curve. The homoclinic orbits from three locations on the curve ho, indicated by filled circles, are shown in Fig. 7.

$u > 0$ corresponds to a periodic orbit in the truncated normal form. In the same spirit, a Neimark–Sacker bifurcation and a torus in the truncated normal form equations appear as, respectively, a Hopf bifurcation and a periodic orbit in the truncated amplitude equations.

The invariant torus, created when the periodic orbit crossed the ns curve, blows up and eventually touches both equilibria. This happens on the curve hc (see Fig. 4), and creates a second heteroclinic connection between the equilibria. The second connection corresponds to a spherelike surface in the full (truncated) normal form. Together with heteroclinic connection on the y-axis, it forms a heteroclinic cycle between the two equilibria. In Fig. 5, this cycle is drawn in three dimensions.

The bifurcation scenario sketched in Figs. 4 and 5 is valid for the *truncated* normal-form equations (4.3). Since in practice we always deal with systems in which higher-order, perturbative terms show up when carrying out the normalization, the effect of such perturbations [the $O(|y, z, \overline{z}|^4)$ terms in Eq. (4.2)] must be considered. The perturbations do not affect the local bifurcations (saddle-node, Hopf, Neimark–Sacker) but they perturb the heteroclinic connections. For instance, the connection on the y-axis is due to the invariance of that axis, since in the truncated normal form (4.3) $\dot{u}$ is proportional to u. However, the higher-order perturbations can contain terms proportional to y^{4+l}, $l \in \mathbb{N}$, that destroy the invariance and thereby the connection. In other words, the perturbations break the symmetry of the truncated normal form.

The heteroclinic cycle will, in general, be destroyed by the perturbations, leaving instead two homoclinic orbits. These are attached to either one of the two fixed points and stretch toward the other equilibrium. An example is shown in Fig. 5. The homoclinic orbit resembles the former heteroclinic cycle but does not reach all the way to the second equilibrium. The other orbit, attached to the lower equilibrium and stretching toward the upper one, is not shown. In some cases the homoclinic orbits can be of the Shil'nikov type, implying the
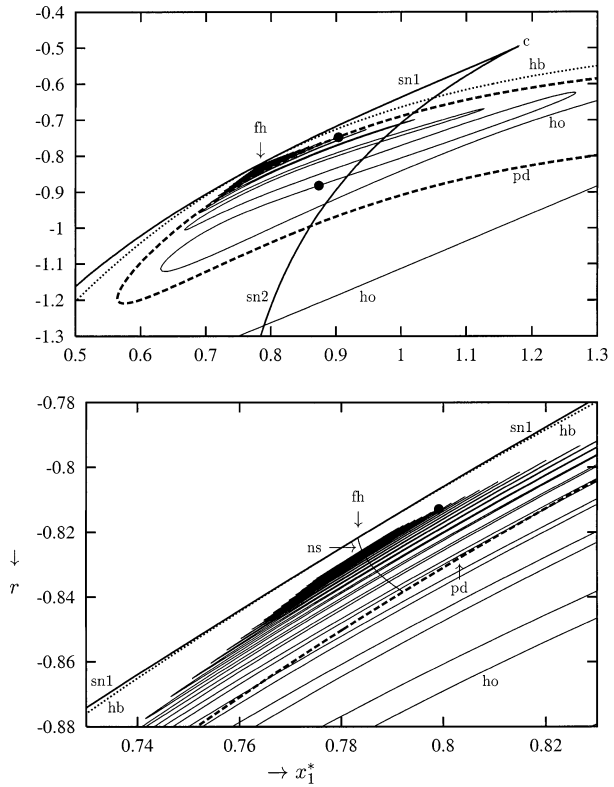
presence of a chaotic invariant set. As the issue of chaotic behavior is not our focus here, we do not explore this possibility.

c. Numerical bifurcation analysis

Figure 6 shows the results of the numerical bifurcation analysis of the model equations (2.6). The calculations were done using AUTO. The orographic height was decreased to $\gamma = 0.2$ for the calculation, corresponding to a topography amplitude of 200 m (instead of 1 km when $\gamma = 1$). This is more realistic than $\gamma = 1$, since the individual spectral components (see section 2) of realistic topography will have amplitudes (much) smaller than the original topography itself [see, e.g., Charney et al. (1981), where topographic maxima of about 2 km result in spectral amplitudes of a few hundred meters or less]. Moreover, a decrease of γ will shift the region of multiple equilibria to more realistic physical values. We will come back to this in the next section. A value of 0.2 for γ results, as could have been

predicted from Fig. 3, in a cusp bifurcation (c) at $(x_1^*, r) = (1.178645, -0.4965761)$, in which the two saddle-node bifurcation curves (sn1 and sn2) coincide. This implies that when $\gamma = 0.2$, only one equilibrium is found if there is no forcing in the second zonal mode (i.e., $r = 0$).

The numerical analysis recovers the theoretically predicted phenomena sketched in the previous section. The Hopf curve (hb) becomes tangent to sn1 in the fold-Hopf bifurcation point fh at $(x_1^*, r) = (0.783\,324, -0.821\,677)$. The eigenvalue spectrum at this bifurcation point is $(0, \pm i0.293\,756, -0.103\,994, -0.248\,003 \pm i0.206\,738)$. Thus, locally in phase space the system is attracted toward the center manifold associated with the fh bifurcation. From the fh point the Neimark–Sacker curve (ns) can be seen to originate (Fig. 6, bottom). The ns curve ends on the curve of the first period-doubling bifurcation (pd). This pd curve is not predicted by the unfolding of the fold-Hopf bifurcation, as it is not in the immediate parameter neighborhood of the fh point. The period doubling is encountered when following the periodic orbit born on the hb curve into the parameter plane. It is the first of what is probably a cascade of period doublings. In Shil'nikov et al. (1995) and Van Veen (2004), similar (but more detailed) bifurcation analyses are presented in the context of the Lorenz-84 baroclinic model.

As has been explained, the unfolding of the truncated normal form of the fold-Hopf bifurcation contains a heteroclinic bifurcation curve on which a heteroclinic cycle exists that connects the two equilibria eq1 and eq2. The cycle will be broken under perturbations, leaving homoclinic orbits that are nearly heteroclinic cycles. One of these orbits is found numerically by continuation of the periodic orbit created on the curve hb. Starting the continuation in r of the periodic orbit born on hb at $x_1^* = 0.9$, the orbit becomes homoclinic to the upper equilibrium eq1 at $r = -1.188\,582$. During the continuation, the first period-doubling curve pd is crossed twice. By continuation of the homoclinic bifurcation, a curve is obtained that winds in toward the point fh. In Fig. 6 this curve is denoted ho. Note that part of the curve falls beyond the limits of the upper figure. The two segments in the figure are connected via a turning point at $(x_1^*, r) = (1.806\,245, -0.517\,351\,3)$. When the curve approaches the fh point, its windings are very close to each other and calculation becomes increasingly harder. Therefore, the continuation of the ho curve does not reach all the way to the fh point, although that is where the curve can be expected to really end. The second homoclinic curve, not shown in Fig. 6, also winds in toward the fh point. It intersects the first homoclinic curve ho infinitely many times near fh. The orbits on this second curve are homoclinic to eq2.

In order to show that the homoclinic orbits indeed become nearly heteroclinic cycles near fh, three orbits taken from curve ho are depicted in Fig. 7 (see also Fig. 6, where the three locations on the ho curve are
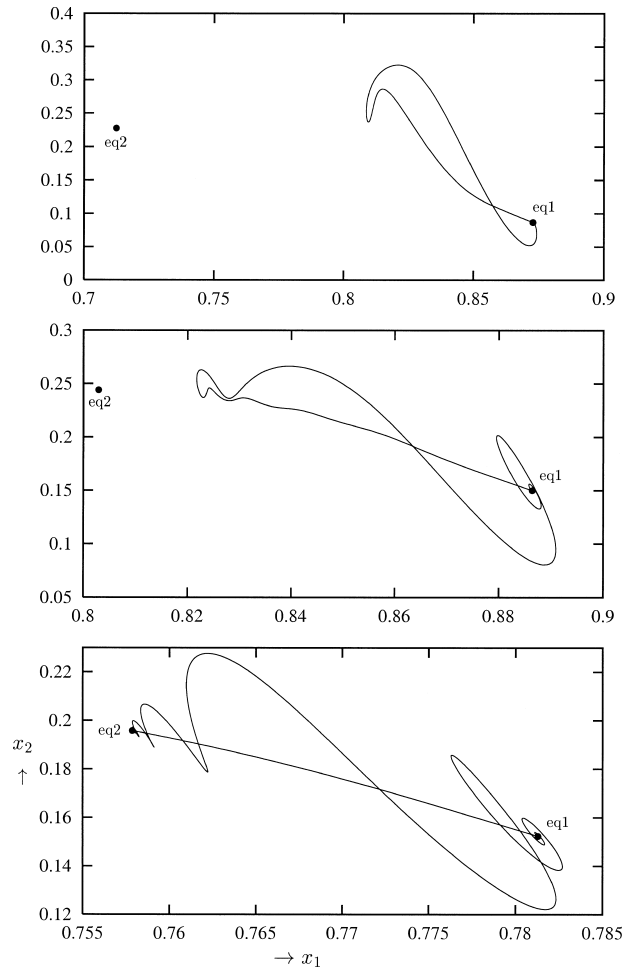

FIG. 7. Homoclinic orbits at various points on the homoclinic curve ho. The orbits are all attached to the zonal equilibrium eq1 and can be seen to approach the wavelike equilibrium eq2 when moving along the curve ho toward the fold-Hopf point.

indicated by a filled circle). The first is the orbit that exists at $(x_1^*, r) = (0.873\,867\,4, -0.881\,582\,7)$. This is still quite far from the fold-Hopf point. The orbit is attached to the zonal equilibrium eq1 and can be seen to tend toward the second, wavelike equilibrium eq2, but does not come very close to it. The second orbit, with $(x_1^*, r) = (0.903\,724\,0, -0.747\,400\,2)$, tends more clearly to eq2. The third orbit, $(x_1^*, r) = (0.799\,150\,1, -0.812\,858\,9)$, comes very close to the second equilibrium and almost forms a heteroclinic cycle. In Fig. 8, this nearly heteroclinic cycle is plotted in various projections. They suggest that one part of the cycle runs over a spherelike surface, while the other part is approximately an axis through the middle of that sphere. This is in agreement with the theoretical picture, see Fig. 5. A similar structure showed up in an EOF-based atmosphere model studied in Crommelin (2002).

The structure of fixed points, periodic orbits, and connections arising out of the fold-Hopf bifurcation induces several periodicities in the system. The unstable and
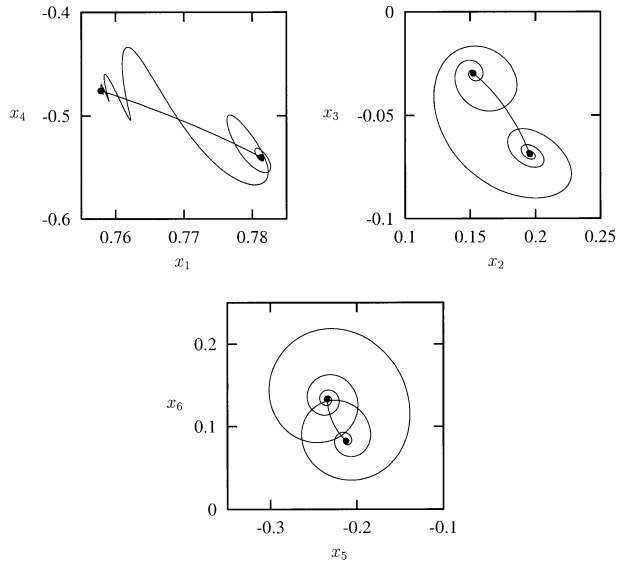
FIG. 8. Nearly heteroclinic cycle in various projections.

stable leading complex eigenmodes of eq1 and eq2, respectively, each have an oscillation period. These oscillations are not related to periodic orbits (although it is possible that in a more complex situation periodic orbits will be thrown off by eq1 or eq2, due to new Hopf bifurcations). Also, the primary periodic orbit born on the Hopf curve hb is an essential element in the unfolding of the fold-Hopf bifurcation. Furthermore, the torus created in the Neimark–Sacker bifurcation is characterized by a second period (the first being, initially, the period of the primary periodic orbit just mentioned). This second period is likely to be highly variable in parameter space, as the torus may be destroyed or touch the equilibria. Finally, the orbits homoclinic to eq1 and eq2 will give rise to either an infinity of periodic orbits (in the case of a Shil'nikov-type homoclinic bifurcation) or one unique periodic solution (in the other case). For mathematical details of the periodic orbits generated by homoclinic bifurcations, see Kuznetsov (1995). See also Van Veen (2004) for a detailed analysis of the relation between the homoclinic bifurcation and the period-doubling cascade. In Tuwankotta (2002) heteroclinic behavior is analyzed in a general three-dimensional system with quadratic, norm-preserving nonlinearities.

5. Bimodality

Numerical integration of the system, in order to see the influence of the fold-Hopf bifurcation, is complicated by the presence of the stable equilibrium eq3. In the parameter range under consideration (see Fig. 6), this fixed point does not become unstable. However, if we inspect the behavior just beyond the second saddle-node curve sn2, eq3 does not exist anymore but its former presence still generates a stagnation point for the system. The role of such stagnation points in regime

behavior, also called "ghost equilibrium" points or "quasi-stationary" states, is discussed in Legras and Ghil (1985) and studied in detail in Mukougawa (1988). If we integrate the system at $(x_1^*, r) = (0.95, -0.801)$, a point in parameter space close to the homoclinic bifurcation curve ho and just beyond sn2 (which is at $x_1^* = 0.945$ when $r = -0.801$), regime behavior is visible. That is, the system alternately visits the neighbourhoods of eq1 and (the former location of) eq2 and eq3.

The results of an integration of 4000 time units (equivalent to 4000 days) are shown in Fig. 9. Plotting x_1 versus time, we see lingering around and transiting between eq1 on the one hand and the former location of eq2 and eq3 on the other hand. Also shown is a projection of the integration orbit onto the (x_1, x_4) plane. Comparing with Fig. 8, one sees that the trajectories of the system have grown in phase space extent, but still follow roughly the same route as the nearly heteroclinic cycle in Fig. 8. The probability density function (pdf) of the distribution of states in the (x_1, x_4) plane shows two maxima toward the far ends of the elongated structure. This is the imprint of the regime behavior on the pdf. The high phase speed of the system during its oscillating transition from the zonal to the wavelike equilibrium has the effect that states from these transitions are hardly visible in the pdf.

The system trajectory can be seen to turn around before really reaching the fixed points. It causes the pdf maxima to lie closer to the time-mean state of the system than the fixed points. This has been observed elsewhere (Reinhold and Pierrehumbert 1982; Achatz and Opsteegh 2003): the anomaly patterns of the regimes are similar to those of the fixed points, but the amplitudes of the regime anomalies are smaller. In Fig. 10, the flow patterns corresponding to eq1 at $(x_1^*, r) = (0.95, -0.801)$ and to eq2 and 3 at $(x_1^*, r) = (0.945, -0.801)$ (the saddle-node bifurcation point sn2, where eq2 and eq3 collide) are shown. In dimensional units (using a wind speed scaling $U_0 = 10$ m s^{-1}, related to a channel length of $2\pi \times 10^3$ km), the zonal wind speed reaches a maximum of about 30 m s^{-1} in the jet of the eq1 pattern. In the eq2 and 3 pattern it is about 25 m s^{-1}. These are surprisingly realistic values, especially when compared to the jet speed maxima of 150 m s^{-1} or more, usually seen for this type of model. It results from the decrease of the topographic height (0.2 instead of 1.0 km), which causes the region of parameter space with multiple equilibria to be located at more realistic values of the forcing parameters. Thus, the almost classical objection of unrealistically strong jets, raised against CDV-like studies in, for example, Tung and Rosenthal (1985), does not hold for our choice of parameters.

To get an impression of the strength of the forcing the model is exposed to in the preceding integration, the forcing profile ψ^* corresponding to $(x_1^*, r) = (0.95, -0.801)$ is converted to the zonal velocity forcing profile $u = -\partial \psi^*/\partial y$. The resulting dimensional profile,
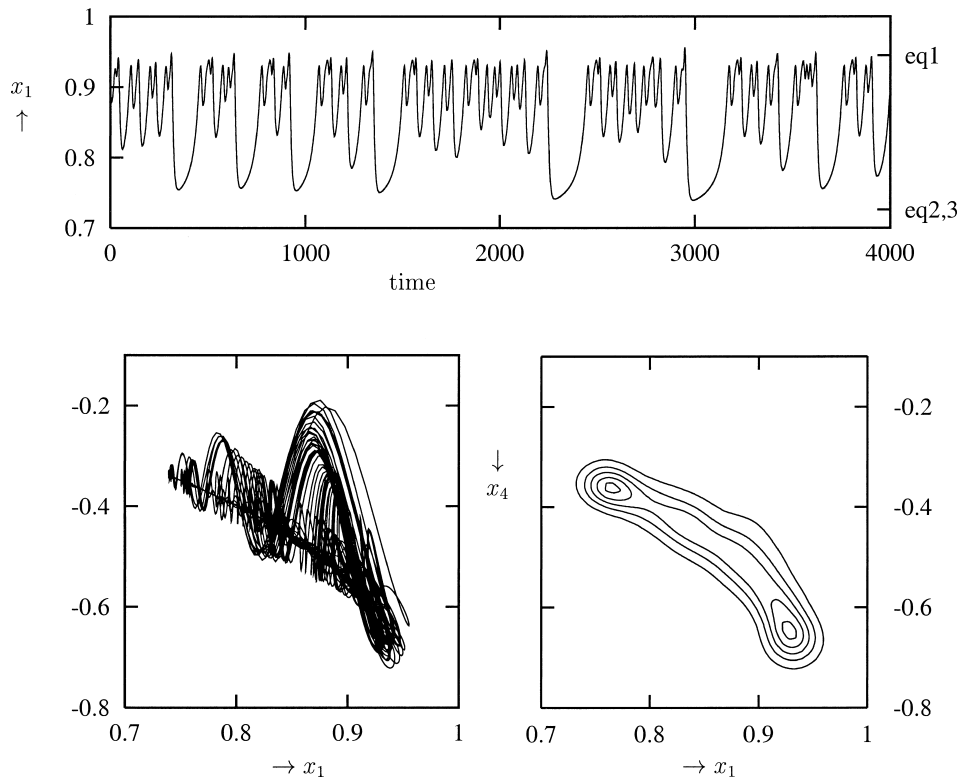
FIG. 9. Results of a 4000-day integration at $(x_1^*, r) = (0.95, -0.801)$. (top) x_1 vs time. The x_1 values of eq1 and of the previous location of eq2 and eq3 (see text) are indicated. (bottom left) Projection of integration data onto (x_1, x_4) plane. (bottom right) The pdf in (x_1, x_4) plane calculated from integration data.

using again the scaling of $U_0 = 10$ m s^{-1}, is shown in Fig. 11. Also plotted there is the forcing profile corresponding to the fold-Hopf bifurcation point $(x_1^*, r) = (0.783\ 324, -0.821\ 677)$. The maximum velocity in the jet in the northern half of the domain is about 30 m s^{-1}

for the forcing used in the integration, and 25 m s^{-1} for the forcing in the fold-Hopf bifurcation. These values are in the range of the velocities reached by the tropospheric jet in the real atmosphere.

In the previous section, the occurrence of several periodicities, associated with the unfolding of the fold-Hopf bifurcation, was discussed. For the integration parameter settings, $(x_1^*, r) = (0.95, -0.801)$, the zonal
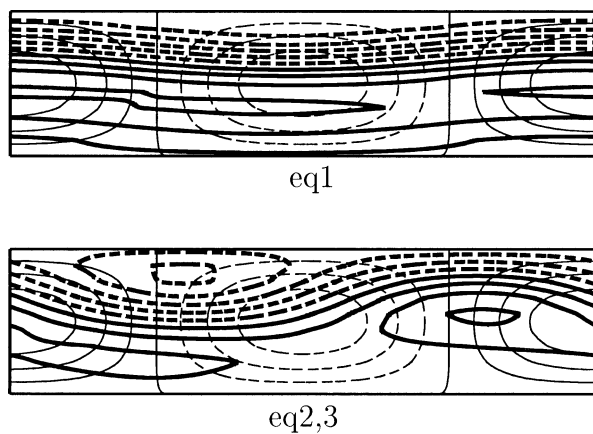

FIG. 10. Flow regimes corresponding to (top) eq1 at $(x_1^*, r) = (0.95, -0.801)$ and (bottom) to eq2 and 3 at the point where they collide [the saddle-node point sn2 at $(x_1^*, r) = (0.945, -0.801)$]. Thick lines are streamfunction lines (contour interval 0.2 in nondimensional units), thin lines are topography contours (interval 0.05 km). Dashed lines/contours are for negative values; solid lines/contours for zero or positive values.
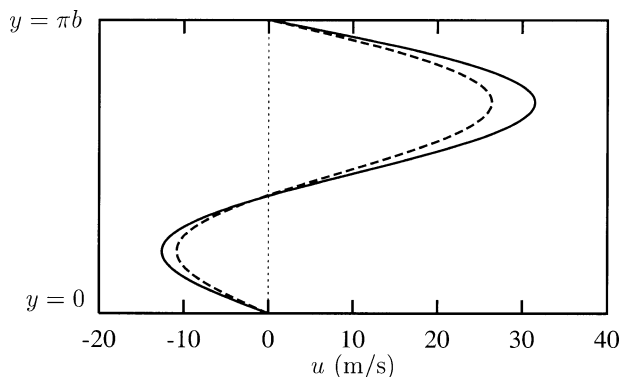

FIG. 11. Meridional dependence of forcing profile ψ^*, converted to zonal wind speed u in m s^{-1}. Profile corresponding to $(x_1^*, r) = (0.95, -0.801)$, used for the forward integration in section 5 (solid line). Profile corresponding to fold-Hopf bifurcation point at $(x_1^*, r) = (0.783\ 324, -0.821\ 677)$ (dashed line).

equilibrium eq1 has a complex pair ($0.247\,140 \pm i0.315\,545$) as its only unstable eigenvalues. The oscillation period corresponding to this eigenvalue pair is about 20 days. The period related to the stable leading eigenmode of eq2 just before sn2 at $(x_1^*, r) = (0.945, -0.801)$, is about 9 days. The principal periodic orbit, born on the curve hb, has a period of 18 days at $(x_1^*, r) = (0.95, -0.801)$. The second period of the torus is not recognizable; the torus may very well not exist anymore for these parameter values. A typical period associated with the switching between the regimes does not exist anymore, due to the irregular nature of the regime switching.

6. Conclusions

The purpose of the work presented in this paper was to isolate and study a specific mechanism that can generate regime transitions in an atmosphere model that has no noise terms. The mechanism involves the simultaneous occurrence, in a realistic parameter range, of barotropic and topographic instability in a so-called fold-Hopf bifurcation. Due to this bifurcation, phase space connections are created that allow for transitions between flow regimes. These transitions are deterministic (in the sense that they are not noise-induced but instead generated by a completely deterministic model) but not necessarily predictable, due to possible chaotic behavior (as in Fig. 9). The aim of this work was not to study or simulate regime transitions in considerably realistic detail; caution is therefore warranted when applying or extrapolating the results to the real atmosphere or to complex atmosphere models. The applicability of these results rests primarily on the fact that the presence of orography and a barotropically unstable jet is a combination that is both realistic and by itself capable of generating regime transitions. Moreover, the values for the topographic heights and atmospheric jet speeds in this paper are in a realistic range. Thus, the mechanism studied here may play a role in generating regime transitions in complex models or in the real atmosphere. We do not claim that the precise shapes of the phase space connections found in this study should be very similar to those in complex models or in reality.

The normal-form equations, associated with the fold-Hopf bifurcation, describe the dynamics of the system restricted to the center manifold. Truncating the normal-form equations after their cubic terms yields a system which needs the tuning of only one parameter to have a heteroclinic cycle among its solutions. The truncated normal-form equations are S^1-symmetric, which explains the low codimensionality of the cycle [see Krupa (1997) for the relation between symmetries and heteroclinic cycles]. This symmetry (or near symmetry, for the nontruncated system) is made explicit by the normalization, and is a hidden symmetry of the nonnormalized system.

The heteroclinic cycle consists of connections back and forth between two steady states. For the model studied in this paper, one of these steady states represents a situation of dominant zonal flow, the other an equilibrium flow with a mainly wavelike character. The fold-Hopf bifurcation and its unfolding thus provide a scenario in which regime transitions can be related to heteroclinic connections.

Since in a natural system perturbative terms will always be present in the model equations, the heteroclinic cycle will be broken. Two homoclinic orbits are left (in general with different stability properties), each attached to one of the involved equilibria. The curves of the two homoclinic bifurcations extend quite far into parameter space. Their existence is not limited to the immediate parameter neighborhood of the fold-Hopf point (see Fig. 6). Near the fh point the homoclinic orbits are nearly heteroclinic cycles, farther away they still tend toward the unconnected second fixed point without coming really close. This dynamical configuration can explain why regime behavior often tends to favor one regime over the other, an explanation previously speculated on in Crommelin (2003b).

The crucial ingredients for the dynamical structure described in this paper are saddle-node and Hopf bifurcations. The occurrence of such bifurcations are certainly no model artifacts, but on the contrary very generic features in atmosphere models. In the model studied here, the presence of topography creates saddle-node bifurcations, whereas Hopf bifurcations are the result of barotropic instability. In more complex models, the number of bifurcations will increase, not decrease, as, for example, many more topographic spectral components will be present (thereby increasing the number of saddle-node bifurcations). Moreover, the inclusion of baroclinic dynamics will add a new source of instabilities and thus increase the number of Hopf bifurcations. Having a considerable number of saddle-node and Hopf bifurcations around, it should not be too hard to have two of them merge into a fold-Hopf bifurcation by tuning two of the available parameters. Thus, in complex models, fold-Hopf bifurcations are likely to be present. However, since the behavior of these models will be complicated by many other phenomena, the central role of fold-Hopf points in more complex models remains to be assessed.

Note that the model does not need to be drawn exactly to the parameter values of the fold-Hopf bifurcation (or to a very narrow parameter range surrounding the bifurcation point) to still "feel" the presence of this bifurcation. The fold-Hopf bifurcation itself is a codimension 2 phenomenon, that is, it occupies only a point in a two-dimensional parameter plane (or a curve in a three-dimensional parameter space), but its influence stretches far beyond the immediate vicinity of that point. See, for instance, the top panel of Fig. 6: the homoclinic bifurcation curve (ho) that emanates from the fold-Hopf point varies over a large range of parameter values. Also, the integration shown in Fig. 9 clearly still bears

the characteristics of the heteroclinic cycle, but was made with parameter values corresponding to a roughly 20% stronger forcing when compared to the fold-Hopf point (see also Fig. 11).

The existence of multiple equilibria in this model is an effect of the zonal resonance brought about by a waveguiding effect due to the channel geometry and severe truncation of the model. One may wonder what will be left of the zonal resonance and multiple equilibria in more complex spherical models. A study by Yang et al. (1997) shows that not all is lost once the Rossby wave dispersion due to spherical geometry enters the stage. This study points out that baroclinic processes can have a waveguide effect that counteracts the Rossby wave dispersion. Thus, the waveguide effect in the barotropic channel model is not completely artificial but rather mimics the waveguiding of the more complex baroclinic spherical models.

The general idea that regime transitions are related to heteroclinic cycles would be "falsified" (or at least not be very useful) if transitions in complex models or in the real atmosphere would not show any sign of preferred transition paths through phase space. For a moderately complex model, preferred transition routes were shown to exist in an earlier study (Crommelin 2003b). The existence of preferred transition paths in the real atmosphere is presently under study; preliminary results can be found in Crommelin (2003a) and suggest that such preferences indeed exist. More specifically, checking whether the interaction of barotropic and topographic instabilities is indeed responsible for the creation of a cycle can be done by either carrying out a numerical bifurcation analysis of more complex models, or by using weakly nonlinear analysis, the common tool of analyzing models with heteroclinicike behavior.

REFERENCES

Achatz, U., and J. D. Opsteegh, 2003: Primitive-equation-based low-order models with seasonal cycle. Part II: Application to complexity and nonlinearity of large-scale atmosphere dynamics. *J. Atmos. Sci.,* **60,** 478–490.

Benzi, R., A. R. Hansen, and A. Sutera, 1984: On stochastic perturbations of simple blocking models. *Quart. J. Roy. Meteor. Soc.,* **110,** 393–409.

——, P. Malguzzi, A. Speranza, and A. Sutera, 1986: The statistical properties of general atmospheric circulation: Observational evidence and a minimal theory of bimodality. *Quart. J. Roy. Meteor. Soc.,* **112,** 661–674.

Charney, J. G., and J. G. DeVore, 1979: Multiple flow equilibria in the atmosphere and blocking. *J. Atmos. Sci.,* **36,** 1205–1216.

——, J. Shukla, and K. C. Mo, 1981: Comparison of a barotropic blocking theory with observation. *J. Atmos. Sci.,* **38,** 762–779.

Cheng, X., and J. M. Wallace, 1993: Cluster analysis of the Northern Hemisphere wintertime 500-hPa height field: Spatial patterns. *J. Atmos. Sci.,* **50,** 1205–1216.

Crommelin, D. T., 2002: Homoclinic dynamics: A scenario for atmospheric ultralow-frequency variability. *J. Atmos. Sci.,* **59,** 1533–1549.

——, 2003a: Nonlinear dynamics of atmospheric regime transitions. Ph.D. thesis, Utrecht University, 127 pp.

——, 2003b: Regime transitions and heteroclinic connections in a barotropic atmosphere. *J. Atmos. Sci.,* **60,** 229–246.

Cushman-Roisin, B., 1994: *Introduction to Geophysical Fluid Dynamics.* Prentice-Hall, 320 pp.

De Swart, H. E., 1988a: Low-order spectral models of the atmospheric circulation: A survey. *Acta Appl. Math.,* **11,** 49–96.

——, 1988b: Vacillation and predictability properties of low-order atmospheric spectral models. Ph.D. thesis, Utrecht University, 121 pp.

——, 1989: Analysis of a six-component atmospheric spectral model: Chaos, predictability and vacillation. *Physica D,* **36,** 222–234.

——, and J. Grasman, 1987: Effect of stochastic perturbations on a low-order spectral model of the atmospheric circulation. *Tellus,* **39A,** 10–24.

Doedel, E. J., and X. J. Wang, 1995: AUTO94: Software for continuation and bifurcation problems in ordinary differential equations. Center for Research on Parallel Computing Tech. Rep. CRPC-95-2, California Institute of Technology, 67 pp.

Egger, J., 1981: Stochastically driven large-scale circulations with multiple equilibria. *J. Atmos. Sci.,* **38,** 2606–2618.

Itoh, H., and M. Kimoto, 1996: Multiple attractors and chaotic itinerancy in a quasigeostrophic model with realistic topography: Implications for weather regimes and low-frequency variability. *J. Atmos. Sci.,* **53,** 2217–2231.

——, and ——, 1997: Chaotic itinerancy with preferred transition routes appearing in an atmospheric model. *Physica D,* **109,** 274–292.

——, and ——, 1999: Weather regimes, low-frequency oscillations, and principal patterns of variability: A perspective of extratropical low-frequency variability. *J. Atmos. Sci.,* **56,** 2684–2705.

Källén, E., 1981: The nonlinear effects of orographic and momentum forcing in a low-order, barotropic model. *J. Atmos. Sci.,* **38,** 2150–2163.

——, 1982: Bifurcation properties of quasi-geostrophic, barotropic models and their relation to atmospheric blocking. *Tellus,* **34,** 255–265.

Kimoto, M., and M. Ghil, 1993a: Multiple flow regimes in the Northern Hemisphere winter. Part I: Methodology and hemispheric regimes. *J. Atmos. Sci.,* **50,** 2625–2643.

——, and ——, 1993b: Multiple flow regimes in the Northern Hemisphere winter. Part II: Sectorial regimes and preferred transitions. *J. Atmos. Sci.,* **50,** 2645–2673.

Krupa, M., 1997: Robust heteroclinic cycles. *J. Nonlinear Sci.,* **7,** 129–176.

Kuo, H. L., 1949: Dynamic instability of two-dimensional nondivergent flow in a barotropic atmosphere. *J. Meteor.,* **6,** 105–122.

Kuznetsov, Yu. A., 1995: *Elements of Applied Bifurcation Theory.* Springer-Verlag, 515 pp.

——, 1999: Numerical normalization techniques for all codim 2 bifurcations of equilibria in ODE's. *SIAM J. Numer. Anal.,* **36,** 1104–1124.

——, and V. V. Levitin, cited 1997: CONTENT: A multiplatform environment for analyzing dynamical systems. Dynamical Systems Laboratory, Centrum voor Wiskunde en Informatica, Amsterdam. [Available online at ftp://ftp.cwi.nl/pub/CONTENT.]

Legras, B., and M. Ghil, 1985: Persistent anomalies, blocking and variations in atmospheric predictability. *J. Atmos. Sci.,* **42,** 433–471.

Mo, K. C., and M. Ghil, 1987: Statistics and dynamics of persistent anomalies. *J. Atmos. Sci.,* **44,** 877–901.

——, and M. Ghil, 1988: Cluster analysis of multiple planetary flow regimes. *J. Geophys. Res.,* **93,** 10 927–10 952.

Molteni, F., S. Tibaldi, and T. N. Palmer, 1990: Regimes in the wintertime circulation over northern extratropics. I: Observational evidence. *Quart. J. Roy. Meteor. Soc.,* **116,** 31–67.

Monahan, A. H., L. Pandolfo, and J. C. Fyfe, 2001: The preferred structure of variability of the Northern Hemisphere atmospheric circulation. *Geophys. Res. Lett.,* **28,** 1019–1022.

Mukougawa, H., 1988: A dynamical model of ''quasi-stationary'' states in large-scale atmospheric motions. *J. Atmos. Sci.,* **45,** 2868–2888.

Namias, J., 1950: The index cycle and its role in the general circulation. *J. Meteor.,* **7,** 130–139.

Plaut, G., and R. Vautard, 1994: Spells of low-frequency oscillations and weather regimes in the Northern Hemisphere. *J. Atmos. Sci.,* **51,** 210–236.

Reinhold, B. B., and R. T. Pierrehumbert, 1982: Dynamics of weather regimes: Quasi-stationary waves and blocking. *Mon. Wea. Rev.,* **110,** 1105–1145.

Rex, D. F., 1950a: Blocking action in the middle troposphere and its effect on regional climate. I. An aerological study of blocking action. *Tellus,* **2,** 196–211.

——, 1950b: Blocking action in the middle troposphere and its effect on regional climate. II. The climatology of blocking action. *Tellus,* **2,** 275–301.

Shil'nikov, A., G. Nicolis, and C. Nicolis, 1995: Bifurcation and predictability analysis of a low-order atmospheric circulation model. *Int. J. Bifurcation Chaos,* **5,** 1701–1711.

Smyth, P., K. Ide, and M. Ghil, 1999: Multiple regimes in Northern Hemisphere height fields via mixture model clustering. *J. Atmos. Sci.,* **56,** 3704–3723.

Sura, P., 2002: Noise-induced transitions in a barotropic β-plane channel. *J. Atmos. Sci.,* **59,** 97–110.

Sutera, A., 1986: Probability density distribution of large-scale atmospheric flow. *Advances in Geophysics,* Vol. 29, Academic Press, 227–249.

Tian, Y., E. R. Weeks, K. Ide, J. S. Urbach, C. N. Baroud, M. Ghil, and H. L. Swinney, 2001: Experimental studies of an eastward jet over topography. *J. Fluid Mech.,* **438,** 129–157.

Tung, K. K., and A. J. Rosenthal, 1985: Theories of multiple equilibria—A critical reexamination. Part I: Barotropic models. *J. Atmos. Sci.,* **42,** 2804–2819.

Tuwankotta, J. M., 2002: Higher order resonances in dynamical systems. Ph.D. thesis, Utrecht University, 136 pp.

Van Veen, L., 2004. Baroclinic flow and the Lorenz-84 model. *Int. J. Bifurcation Chaos,* in press.

Weeks, E. R., Y. Tian, J. S. Urbach, K. Ide, H. L. Swinney, and M. Ghil, 1997: Transitions between blocked and zonal flows in a rotating annulus with topography. *Science,* **278,** 1598–1601.

Yang, S., B. Reinhold, and E. Källén, 1997: Multiple weather regimes and baroclinically forced spherical resonance. *J. Atmos. Sci.,* **54,** 1397–1409.

Yoden, S., 1985: Bifurcation properties of a quasi-geostrophic, barotropic, low-order model with topography. *J. Meteor. Soc. Japan,* **63,** 535–546.